Journal of Controlled Release 360 (2023) 225–235

Contents lists available at ScienceDirect

Journal of Controlled Release

journal homepage: www.elsevier.com/locate/jconrel

Controlling release from encapsulated drug-loaded devices: insights from modeling the dissolution front propagation

Ankur Jain [a,*], David King [b], Giuseppe Pontrelli [c], Sean McGinty [d,e,**]

[a] Mechanical and Aerospace Engineering Department, University of Texas at Arlington, Arlington, TX, USA
[b] School of Mathematics & Statistics, University of Glasgow, Glasgow, UK
[c] Istituto per le Applicazioni del Calcolo – CNR Via dei Taurini 19, Rome 00185, Italy
[d] Division of Biomedical Engineering, University of Glasgow, Glasgow, UK
[e] Glasgow Computational Engineering Centre, University of Glasgow, Glasgow, UK

ARTICLE INFO

Keywords:
Dissolution
Diffusion
Drug delivery devices
Drug release profile
Dissolution front propagation

ABSTRACT

Dissolution of drug from its solid form to a dissolved form is an important consideration in the design and optimization of drug delivery devices, particularly owing to the abundance of emerging compounds that are extremely poorly soluble. When the solid dosage form is encapsulated, for example by the porous walls of an implant, the impact of the encapsulant drug transport properties is a further confounding issue. In such a case, dissolution and diffusion work in tandem to control the release of drug. However, the interplay between these two competing processes in the context of drug delivery is not as well understood as it is for other mass transfer problems, particularly for practical controlled-release considerations such as an encapsulant layer around the drug delivery device. To address this gap, this work presents a mathematical model that describes controlled release from a drug-loaded device surrounded by a passive porous layer. A solution for the drug concentration distribution is derived using the method of eigenfunction expansion. The model is able to track the dissolution front propagation, and predict the drug release curve during the dissolution process. The utility of the model is demonstrated through comparison against experimental data representing drug release from a cylindrical drug-loaded orthopedic fixation pin, where the model is shown to capture the data very well. Analysis presented here reveals how the various geometrical and physicochemical parameters influence drug dissolution and, ultimately, the drug release profile. It is found that the non-dimensional initial concentration plays a key role in determining whether the problem is diffusion-limited or dissolution-limited, whereas the nature of the problem is largely independent of other parameters including diffusion coefficient and encapsulant thickness. We expect the model will prove to be a useful tool for those designing encapsulated drug delivery devices, in terms of optimizing the design of the device to achieve a desired drug release profile.

1. Introduction

A sound understanding of drug dissolution [1–3] is of fundamental importance in the design and optimization of controlled release technologies [4–6]. This is particularly true for the case of drugs that are loaded in a solid form, since the drug is required to dissolve before it can be readily transported and exert its therapeutic effect [5]. The process of dissolution has attracted the interest of scientists from a wide range of backgrounds for well over a century, dating back to the 1800s, when Noyes and Whitney presented the first semi-empirical model of dissolution [7]. In subsequent years, several authors presented alternative semi-empirical models, attempting to shed light on the underlying physical mechanisms of the process [8–10]. Dissolution has remained a topic of much research interest, with experimental investigation and mathematical modeling of underlying physical processes both needed to facilitate greater understanding of controlled drug release. Mathematical approaches in particular hold many advantages, including but not limited to: identifying the relative importance of system parameters in governing the dissolution/drug release rate; helping guide the design, and reducing the number of experiments and; contributing towards minimizing the cost and time associated with physical measurements.

In the past few decades, increasingly complex mathematical models of dissolution have been presented, attempting to provide more accurate

* Correspondence to: A. Jain, 500 W First St, Rm 211, Arlington, TX 76019, USA.
** Correspondence to: S. McGinty, James Watt South Building, University Avenue, Glasgow G12 8QQ, UK.
E-mail addresses: jaina@uta.edu (A. Jain), Sean.Mcginty@glasgow.ac.uk (S. McGinty).

https://doi.org/10.1016/j.jconrel.2023.06.019
Received 14 February 2023; Received in revised form 12 June 2023; Accepted 13 June 2023
Available online 26 June 2023

Nomenclature

a	time-varying thickness of the dissolved drug region, measured inwards from the outer surface of drug core (m)
B	initial drug concentration (kg·m^{-3})
c	concentration (kg·m^{-3})
D	diffusion coefficient (m^2·s^{-1})
f	fraction of drug released
h	mass transfer coefficient (m·s^{-1})
r	radial coordinate (m)
R_0	radius of the drug-loaded core (m)
S	solubility limit (kg·m^{-3})
Sh	Sherwood number, $Sh = hR_0/D_f$
t	time (s)
δ	thickness of the porous wall (m)
ξ	non-dimensional spatial coordinate, $\xi = \mathrm{r/R_0}$
ϕ	porosity
τ	non-dimensional time, $\tau = D_f t/R_0^2$
θ	non-dimensional drug concentration, $\theta_i = c_i/S\ (i = f, p)$
Subscripts	
p	porous wall layer
f	drug-loaded core
Overbars	refer to non-dimensional quantities

descriptions of the process [2,11,12]. These may be roughly separated into two types: moving boundary and continuous field descriptions [13]. The moving-boundary approach considers a propagation front that separates dissolved drug from undissolved drug. This has been applied to solid drug formulations [14,15], but has also been considered in the context of solid drug contained with a matrix carrier [8,16,17]. Mass balance at the dissolution interface, i.e., requiring that the rate of drug diffusion away from the dissolution front be balanced by the rate at which the solid drug is dissolved provides a mathematical framework for determining the rate of propagation of the dissolution front. Such front-tracking problems are, in general, non-linear, and several approximate solutions have been proposed. For example, assuming the solid drug concentration to be much larger than the solubility limit, pseudo-steady propagation of the dissolution front has been modeled, resulting in approximate but closed-form solutions for the drug release profile for flat [8] and spherical [18] drug delivery devices. Several other approximate analytical techniques for modeling the propagation of the dissolution front have also been proposed, including integral methods [19] and series expansions [20]. Most recently, an asymptotic expansion of the leading order equations was used to obtain an approximate solution for drug release from a polydisperse granule [16]. Each of the techniques discussed above inherently assume that the dissolution front moves slowly.

The alternative continuous field approach, mostly applied to the case of drug loaded within an inert matrix, obviates the need for a moving boundary by assuming rapid liquid absorption, facilitating dissolution throughout the matrix from the onset [2,21–23]. In other words, the rate of dissolution at any spatial location is assumed to be proportional to the local concentration excess above the solubility limit, following the early Noyes–Whitney [7] and Nernst–Brunner approach [24]. In such a case, the dissolution process results in an additional term in the diffusion eq. [25]. Provided the reaction kinetics parameters are determined correctly, such models hold the advantage of being appropriate for a wider range of solubilities and dissolution rates. Regardless of the model framework, an important, but often overlooked aspect is comparison with experimental data, an essential step if the model is to be used in a predictive capacity.

Most of the past work on dissolution modeling in the context of controlled drug delivery has focused on a homogeneous (so-called *monolithic*) system, such as a slab or sphere, with drug dispersed within. However, there are several scenarios where the drug-loaded region (the *core*) is surrounded or encapsulated by a passive region (the *encapsulant*) whose primary function is to control the release. In particular, drug-filled implants, sized typically of the order of several mm or more, where solid drug is contained within the structure of the implant itself, are emerging in a number of controlled-release applications such as coronary drug-eluting stents [26] and antibiotic-eluting orthopedic implants [27,28]. These devices utilize the hollow core inside the implant as a reservoir for drug delivery without compromising the structural integrity of the implant and obviate the need for polymer carriers which are often associated with biocompatibility issues and and/or delayed healing. In such implants, drug release is typically controlled via a porous wall encapsulating the drug reservoir, with the nature of the pores, and the thickness of the wall being key design parameters. Thus, the diffusion of dissolved drug through the porous wall is an additional factor in determining the overall dissolution and drug release rate that is typically not accounted for by monolithic dissolution models.

The additional complexity of the encapsulating porous wall, exhibiting different diffusion properties from the central core, renders an analytical solution difficult to achieve. However, similar problems occurring in phase change heat transfer [29,30] have been resolved by solving the transient diffusion problem using eigenfunction expansion. Based on this technique, solutions have been derived to model the melting of a spherical phase change material encapsulated within a passive material [29], and melting of a flat slab protected by a multi-layer wall [30]. Given the close similarity between heat and mass transfer, it is conceivable that this technique can also be used to solve a drug dissolution problem in the presence of an encapsulant, and, therefore, address a key gap in the controlled release modeling literature. Doing so will help model multilayer drug delivery devices and understand the interplay between dissolution and diffusion. While such calculations may be carried out successfully using numerical simulations, particularly in complicated geometries [31–34], a theoretical approach may offer advantages of improved computational time [29,30], as well as a deeper fundamental understanding of transport processes and diffusion-vs-dissolution interplay.

This work presents a front-tracking technique for modeling dissolution and the resulting drug release from a drug-loaded cylindrical device surrounded by a passive porous layer. An eigenfunction-based solution for the transient concentration distributions in the two layers is derived, which, along with mass conservation at the dissolution front determines the rate of propagation of the dissolution front. The model is compared against previously reported experimental data encompassing drug release from a cylindrical drug-filled orthopedic fixation pin, and good agreement is found. Key non-dimensional parameters governing this problem are identified, and it is shown that the initial drug concentration plays a key role in determining whether drug release is dissolution-limited, or diffusion-limited.

2. Problem definition

A schematic of the problem considered here is presented in Fig. 1. A cylindrical device of radius R_0 carries a drug within its core at an initial concentration B that is larger than the solubility limit S. The drug core is surrounded by a porous concentric layer of thickness δ. The entire drug delivery device is located in a release medium, into which, the rate of drug delivery is of interest. Dissolution of the solid drug begins when the device is submerged in the release medium at $t = 0$. As time passes, the dissolution front moves inwards, as characterized by the thickness of the dissolved drug region, $a(t)$ measured radially inwards from $r = R_0$. The inward propagation of the dissolution front is driven by outwards diffusion of dissolved drug from the dissolution front towards the release

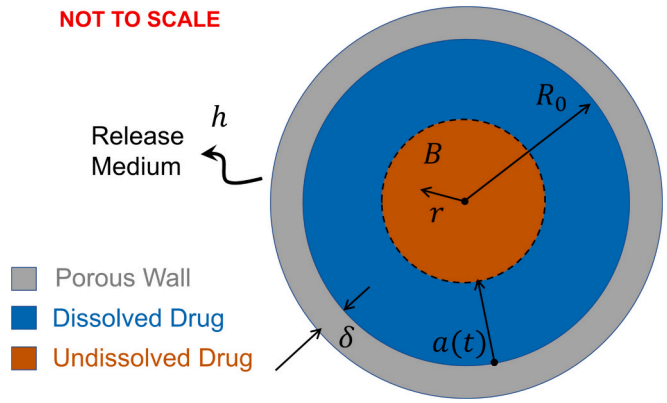

Fig. 1. Transversal cross section schematic of a cylindrical device consisting of a drug-filled core of initial radius R_0 surrounded by a porous wall of thickness δ. The dissolution front, represented by $a(t)$ moves inwards, resulting in onset of diffusion in the dissolved region and the porous wall, and eventually, drug release into the surrounding release medium. h and B denote the mass transfer coefficient to the surrounding release medium and the initial drug concentration, respectively. Figure not to scale.

medium. The interest is in predicting the rate of drug release at the outer surface as a function of time during the dissolution process. Once the dissolution process is complete, i.e., the dissolution front reaches the center of the device, $a = R_0$, further drug delivery is purely diffusive, which is a well-modeled process [35] and therefore, not of interest in this work. Note that in an extreme scenario, depending on the values of various parameters, this problem may be dissolution-limited, in which case, most of the diffusion would already be complete by the time the drug dissolves completely, or diffusion-limited, in which case, dissolution occurs so rapidly that most of the drug is released after the completion of dissolution. With a view to understanding how the drug release may be controlled, it is of interest to examine the conditions in which the process is dissolution-limited or diffusion-limited, and to determine the impact of various problem parameters on the nature of the process.

A number of assumptions, in common with existing drug delivery models, are made in order to solve this problem. Diffusion is assumed to be governed by Fick's second law [35], with isotropic, constant and uniform diffusion coefficients in each layer. The device is assumed to be axisymmetric and capped at both ends, thereby preventing drug release from these areas and ensuring a 1D radial concentration distribution. The drug is assumed to be loaded uniformly within the core. Taken together, these assumptions ensure that the net flux of drug is only in the radial direction towards the release medium, enabling the consideration of a one-dimensional model. It is assumed that the materials do not erode or swell during the dissolution process, the modeling of which would entail solving a problem with two simultaneously moving boundaries. It is also assumed that the drug does not interact with the pore wall during the diffusion process. Further, it is assumed that there are no wettability problems, meaning that the dissolved drug concentration at the dissolution front is equal to the drug solubility. The reader is referred to [36] for alternative models that consider the effect of poorly wettable solids.

Based on the physical description of the problem and assumptions discussed above, the concentration fields in the dissolved region of the core, $c_f(r,t)$, and the surrounding porous region, $c_p(r,t)$, are governed by the following conservation equations written in cylindrical coordinates:

$$\frac{1}{r}\frac{\partial}{\partial r}\left(r\frac{\partial c_f}{\partial r}\right) = \frac{1}{D_f}\frac{\partial c_f}{\partial t}, \qquad R_0 - a(t) < r < R_0, \tag{1}$$

$$\frac{1}{r}\frac{\partial}{\partial r}\left(r\frac{\partial c_p}{\partial r}\right) = \frac{\phi}{D_p}\frac{\partial c_p}{\partial t}, \qquad R_0 < r < R_0 + \delta. \tag{2}$$

Here, ϕ refers to the porosity of the surrounding region. Subscripts f and p refer to the fluid-infused region in the cylindrical core and the surrounding porous region, respectively. Specifically, D_f and D_p refer to the diffusion coefficients in the core and the surrounding porous region, respectively. D_f and D_p are related to each other as $D_p/D_f = \phi_e/\lambda$ where ϕ_e is the effective porosity of the porous wall, which, based on past work may be assumed to be 90% of ϕ, and λ is the tortuosity [37,38], for which, an average value of 3.0 may be assumed [38]. The dissolution front is initially located at R_0, so that initially, $a(0) = 0$ and eventually, $a = R_0$ when all of the drug core has been dissolved. Under this definition, the time-varying radial location of the dissolution front is given by $R_0 - a(t)$.

The above governing equations are supplemented by the following boundary and interface conditions:

$$c_f = S, \qquad r = R_0 - a(t), \tag{3}$$

$$c_f = c_p, \qquad r = R_0, \tag{4}$$

$$-D_f\frac{\partial c_f}{\partial r} = -D_p\frac{\partial c_p}{\partial r}, \qquad r = R_0, \tag{5}$$

$$-D_p\frac{\partial c_p}{\partial r} = hc_p, \qquad r = R_0 + \delta. \tag{6}$$

Eq. (3) states that drug concentration at the dissolution front must be equal to the solubility of the drug. Eqs. (4) and (5) represent continuity of the concentration field and conservation of mass flux at the interface between the cylindrical core and the surrounding porous region. Eq. (6) models the release of the drug into the surrounding medium, assuming drug release governed by the given mass transfer coefficient h. In the special case of an infinitely large release medium, h is infinite and eq. (6) may be replaced with a zero concentration boundary condition, which is typically maintained in *in vitro* experiments.

Since $a(t)$ is not known *a priori*, one further equation is required to fully describe this problem. This may be obtained by considering drug mass conservation at the dissolution front. Over an infinitesimal time dt, the mass of drug released due to the inwards propagation of the drug must be balanced by the outwards diffusive flux away from the front. This is represented mathematically by

$$(B - S)\frac{da}{dt} = -D_f\frac{\partial c_f}{\partial r}, \qquad r = R_0 - a(t), \tag{7}$$

with $a(0) = 0$. Finally, it is assumed that the porous region does not contain any drug at the initial time.

Non-dimensionalization of the equations above reduces the number of parameters and ensures generalization of the results. The following transformation is carried out:

$$\xi = \frac{r}{R_0}, \quad \tau = \frac{D_f t}{R_0^2}, \quad \theta_f = \frac{c_f}{S}, \quad \theta_p = \frac{c_p}{S}, \quad \bar{\delta} = \frac{\delta}{R_0}, \quad \bar{a} = \frac{a}{R_0}, \quad \bar{D}_p = \frac{D_p}{D_f}, \quad \bar{B} = \frac{B}{S}, \quad Sh = \frac{hR_0}{D_f}. \tag{8}$$

Here, $\bar{\delta}$ is the non-dimensional thickness of the porous region, $\bar{a}$ is the non-dimensional thickness of the dissolved drug region, measured inwards from the inner wall of the porous region, $\bar{B}$ is the initial drug concentration in the core relative to its solubility and Sh is the Sherwood number that represents mass transfer to the surrounding medium at the outer surface.

Based on eq. (8), the non-dimensional set of equations that govern this problem may be written as

$$\frac{1}{\xi}\frac{\partial}{\partial \xi}\left(\xi\frac{\partial \theta_f}{\partial \xi}\right) = \frac{\partial \theta_f}{\partial \tau}, \qquad 1 - \bar{a}(\tau) < \xi < 1, \tag{9}$$

$$\frac{1}{\xi}\frac{\partial}{\partial \xi}\left(\xi\frac{\partial \theta_p}{\partial \xi}\right) = \frac{\phi}{\bar{D}_p}\frac{\partial \theta_p}{\partial \tau}, \qquad 1 < \xi < 1 + \bar{\delta}, \tag{10}$$

$$\theta_f = 1, \qquad \xi = 1 - \bar{a}(\tau), \tag{11}$$

$$-\bar{D}_p \frac{\partial \theta_p}{\partial \xi} = Sh\, \theta_p, \qquad \xi = 1 + \bar{\delta}, \tag{12}$$

$$\theta_p = \theta_f, \qquad \xi = 1, \tag{13}$$

$$\bar{D}_p \frac{\partial \theta_p}{\partial \xi} = \frac{\partial \theta_f}{\partial \xi}, \qquad \xi = 1, \tag{14}$$

$$\frac{d\bar{a}}{d\tau} = -\frac{1}{\bar{B}-1}\frac{\partial \theta_f}{\partial \xi}, \qquad \xi = 1 - \bar{a}(\tau). \tag{15}$$

During the drug release process, the two key performance parameters of interest include the thickness of the dissolved region as a function of time, $\bar{a}(\tau)$, and the cumulative amount of drug delivered into the release medium up to a given time, expressed as a fraction of the initial drug mass by

$$\bar{f}(\tau) = \frac{\int_0^t -D_p \left(\frac{\partial c_p}{\partial r}\right)_{1+\delta} 2\pi(R_0+\delta)dt^*}{\pi R_0^2 B} = -\frac{2\bar{D}_p(1+\bar{\delta})\int_0^\tau \left(\frac{\partial \theta_p}{\partial \xi}\right)_{1+\bar{\delta}} d\tau^*}{\bar{B}}. \tag{16}$$

Eqs. (9)-(15) represent a two-layer moving boundary problem driven by the non-homogeneity present in eq. (11). Outwards diffusion of the drug due to the radial concentration results in inwards propagation of the dissolution front until all of the drug core has been dissolved. While an exact analytical solution for such moving boundary problems is usually available only for the simplest problems, such as the Stefan problem [39], an approximate analytical solution may be derived using the method of eigenfunction expansion. This method has been used in the past for analyzing phase change heat transfer problems [30,40,41], including a two-layer problem comprising a phase change material and an encapsulant, similar to the present one [29].

Since the two-layer diffusion problem contains a non-homogeneity in one of the boundary conditions, eq. (11), the solution is first written as a sum of two components:

$$\theta_f(\xi,\tau) = u_f(\xi) + w_f(\xi,\tau), \tag{17}$$

$$\theta_p(\xi,\tau) = u_p(\xi) + w_p(\xi,\tau). \tag{18}$$

where u_f and u_p may be interpreted as the 'steady state' component of the solution. These variables satisfy $\left(\xi u_f'\right)' = 0$ and $\left(\xi u_p'\right)' = 0$, respectively, along with the following boundary conditions:

$$u_f = 1, \qquad \xi = 1 - \bar{a}, \tag{19}$$

$$-\bar{D}_p u_p' = Sh\, u_p, \qquad \xi = 1 + \bar{\delta}, \tag{20}$$

$$u_f = u_p, \qquad \xi = 1, \tag{21}$$

$$\bar{D}_p u_p' = u_f', \qquad \xi = 1. \tag{22}$$

A solution for $u_f(\xi)$ and $u_p(\xi)$ can be easily found to be

$$u_f(\xi) = \bar{D}_p A_p \ln\left(\frac{\xi}{1-\bar{a}}\right) + 1, \tag{23}$$

$$u_p(\xi) = A_p \ln\left(\frac{\xi}{(1-\bar{a})^{\bar{D}_p}}\right) + 1, \tag{24}$$

where

$$A_p = -Sh\left[\frac{\bar{D}_p}{1+\bar{\delta}} + Sh\,\ln\left(\frac{1+\bar{\delta}}{(1-\bar{a})^{\bar{D}_p}}\right)\right]^{-1}. \tag{25}$$

The problem for $w_f(\xi,\tau)$ and $w_p(\xi,\tau)$ may then be written as

$$\frac{1}{\xi}\frac{\partial}{\partial \xi}\left(\xi \frac{\partial w_f}{\partial \xi}\right) = \frac{\partial w_f}{\partial \tau}, \qquad 1-\bar{a} < \xi < 1, \tag{26}$$

$$\frac{1}{\xi}\frac{\partial}{\partial \xi}\left(\xi \frac{\partial w_p}{\partial \xi}\right) = \frac{\phi}{\bar{D}_p}\frac{\partial w_p}{\partial \tau}, \qquad 1 < \xi < 1+\bar{\delta}, \tag{27}$$

$$w_f = 0, \qquad \xi = 1 - \bar{a}, \tag{28}$$

$$-\bar{D}_p \frac{\partial w_p}{\partial \xi} = Sh\, w_p, \qquad \xi = 1 + \bar{\delta}, \tag{29}$$

$$w_f = w_p, \qquad \xi = 1, \tag{30}$$

$$\bar{D}_p \frac{\partial w_p}{\partial \xi} = \frac{\partial w_f}{\partial \xi}, \qquad \xi = 1. \tag{31}$$

The initial conditions for this problem are

$$w_p = -u_p(\xi), \qquad \tau = 0, \tag{32}$$

$$w_f = -u_f(\xi), \qquad \tau = 0. \tag{33}$$

Eqs. (26)-(33) represent a two-layer diffusion problem with homogeneous boundary and interface conditions, and a non-homogeneous initial condition. A solution for this problem may be written as follows:

$$w_f(\xi,\tau) = \sum_{n=1}^{\infty} c_n \left[A_{f,n} \mathrm{J}_0(\lambda_n \xi) + B_{f,n} \mathrm{Y}_0(\lambda_n \xi)\right] \exp\left(-\lambda_n^2 \tau\right), \tag{34}$$

$$w_p(\xi,\tau) = \sum_{n=1}^{\infty} c_n \left[A_{p,n} \mathrm{J}_0\left(\frac{\lambda_n \xi}{\sqrt{\gamma}}\right) + B_{p,n} \mathrm{Y}_0\left(\frac{\lambda_n \xi}{\sqrt{\gamma}}\right)\right] \exp\left(-\lambda_n^2 \tau\right), \tag{35}$$

where λ_n are the eigenvalues and $\gamma = \frac{\bar{D}_p}{\phi}$. J_0 and Y_0 refer to zero-th order Bessel functions of the first and second kind, respectively. Note that the eigenfunctions are chosen to satisfy the respective governing equations. Relationships between $A_{f,n}$ and $B_{f,n}$, and between $A_{p,n}$ and $B_{p,n}$ may be derived on the basis of eqs. (28) and (29), respectively. A relationship between $A_{p,n}$ and $A_{f,n}$ may also be derived using eq. (30). Finally, the substitution of these relationships into eq. (31) may be shown to result in the following simplified form for the solution

$$w_f(\xi,\tau) = \sum_{n=1}^{\infty} c_n \left[\mathrm{J}_0(\lambda_n \xi) + s_{f,n} \mathrm{Y}_0(\lambda_n \xi)\right] \exp\left(-\lambda_n^2 \tau\right), \tag{36}$$

$$w_p(\xi,\tau) = \sum_{n=1}^{\infty} c_n q_{p,n} \left[\mathrm{J}_0\left(\frac{\lambda_n \xi}{\sqrt{\gamma}}\right) + s_{p,n} \mathrm{Y}_0\left(\frac{\lambda_n \xi}{\sqrt{\gamma}}\right)\right] \exp\left(-\lambda_n^2 \tau\right). \tag{37}$$

The eigenvalues λ_n are roots of the following eigenequation

$$\frac{\bar{D}_p}{\sqrt{\gamma}} q_{p,n}\left[\mathrm{J}_1\left(\frac{\lambda_n}{\sqrt{\gamma}}\right) + s_{p,n}\mathrm{Y}_1\left(\frac{\lambda_n}{\sqrt{\gamma}}\right)\right] = \mathrm{J}_1(\lambda_n) + s_{f,n}\mathrm{Y}_1(\lambda_n), \tag{38}$$

where

$$s_{f,n} = -\frac{\mathrm{J}_0(\lambda_n(1-\bar{a}))}{\mathrm{Y}_0(\lambda_n(1-\bar{a}))}, \tag{39}$$

$$s_{p,n} = \frac{\frac{\lambda_n \bar{D}_p}{\sqrt{\gamma}}\mathrm{J}_1\left(\frac{\lambda_n}{\sqrt{\gamma}}(1+\bar{\delta})\right) - Sh\,\mathrm{J}_0\left(\frac{\lambda_n}{\sqrt{\gamma}}(1+\bar{\delta})\right)}{-\frac{\lambda_n \bar{D}_p}{\sqrt{\gamma}}\mathrm{Y}_1\left(\frac{\lambda_n}{\sqrt{\gamma}}(1+\bar{\delta})\right) + Sh\,\mathrm{Y}_0\left(\frac{\lambda_n}{\sqrt{\gamma}}(1+\bar{\delta})\right)}, \tag{40}$$

$$q_{p,n} = \frac{\mathrm{J}_0(\lambda_n) + s_{f,n}\mathrm{Y}_0(\lambda_n)}{\mathrm{J}_0\left(\frac{\lambda_n}{\sqrt{\gamma}}\right) + s_{p,n}\mathrm{Y}_0\left(\frac{\lambda_n}{\sqrt{\gamma}}\right)}. \tag{41}$$

Here, J_1 and Y_1 refer to first order Bessel functions of the first and second kind, respectively.

The last remaining unknown in eqs. (36) and (37), c_n, may be

determined by the use of quasi-orthogonality of a multilayer diffusion problem. In order to do so, one may set $\tau = 0$ in eqs. (36) and (37) and use the initial conditions given by eqs. (32) and (33), respectively. The equations are then multiplied with $\xi\left[\mathrm{J}_0(\lambda_m\xi) + s_{f,m}\mathrm{Y}_0(\lambda_m\xi)\right]$ and $\xi\phi q_{p,m}\left[\mathrm{J}_0\left(\frac{\lambda_m\xi}{\sqrt{\gamma}}\right) + s_{p,m}\mathrm{Y}_0\left(\frac{\lambda_m\xi}{\sqrt{\gamma}}\right)\right]$, respectively, followed by integration within the respective region. Upon adding the resulting equations, with the use of the orthogonality relationship, one may obtain the following expression for c_n:

$$c_n = \frac{-1}{N_n}\left[\int_{1-\bar{a}}^{1} u_f(\xi)\xi\left[\mathrm{J}_0(\lambda_n\xi) + s_{f,n}\mathrm{Y}_0(\lambda_n\xi)\right]d\xi + \phi\int_{1}^{1+\bar{\delta}} \xi u_p(\xi) q_{p,n}\left[\mathrm{J}_0\left(\frac{\lambda_n\xi}{\sqrt{\gamma}}\right) + s_{p,n}\mathrm{Y}_0\left(\frac{\lambda_n\xi}{\sqrt{\gamma}}\right)\right]d\xi\right], \tag{42}$$

where the norm N_n is given by

$$N_n = \int_{1-\bar{a}}^{1} \xi\left[\mathrm{J}_0(\lambda_n\xi) + s_{f,n}\mathrm{Y}_0(\lambda_n\xi)\right]^2 d\xi + \phi\int_{1}^{1+\bar{\delta}} \xi\left[q_{p,n}\left[\mathrm{J}_0\left(\frac{\lambda_n\xi}{\sqrt{\gamma}}\right) + s_{p,n}\mathrm{Y}_0\left(\frac{\lambda_n\xi}{\sqrt{\gamma}}\right)\right]\right]^2 d\xi, \tag{43}$$

This completes the solution for the concentration distribution. Finally, the dissolution front may be obtained by inserting eqs. (23) and (37) into eq. (15), resulting in

$$\begin{aligned}\frac{d\bar{a}}{d\tau} &= -\frac{1}{\bar{B}-1}\left(\frac{\partial\theta_f}{\partial\xi}\right)_{\xi=1-\bar{a}} \\ &= -\frac{1}{\bar{B}-1}\left[\frac{\bar{D}_p A_p}{1-\bar{a}} - \sum_{n=1}^{\infty} c_n\lambda_n\left[\mathrm{J}_1(\lambda_n(1-\bar{a}))\right.\right. \\ &\qquad \left.\left. + s_{f,n}\mathrm{Y}_1(\lambda_n(1-\bar{a}))\right]\exp\left(-\lambda_n^2\tau\right)\right].\end{aligned} \tag{44}$$

Eq. (44) is a relatively simple ordinary differential equation for $\bar{a}(\tau)$. While an analytical integration of eq. (44) is likely not possible, it can be easily numerically integrated, in conjunction with the initial condition $\bar{a}(0) = 0$. An explicit time stepping technique is used, wherein eq. (44) provides the value of $\frac{d\bar{a}}{d\tau}$ at each time in order to determine the value of $\bar{a}$ at the next time step. The time step is chosen to be small enough such that further reduction does not significantly change the results. Once solved, an expression for the fraction of drug delivered into the release medium can be written, using eq. (16) as

$$\bar{f}(\tau) = -\frac{2\bar{D}_p}{\bar{B}}(1+\bar{\delta})\left[\frac{A_p}{1+\bar{\delta}}\tau - \sum_{n=1}^{\infty} c_n q_{p,n}\frac{\lambda_n}{\sqrt{\gamma}}\left(\mathrm{J}_1\left(\frac{\lambda_n}{\sqrt{\gamma}}(1+\bar{\delta})\right) + s_{p,n}\mathrm{Y}_1\left(\frac{\lambda_n}{\sqrt{\gamma}}(1+\bar{\delta})\right)\right)\frac{\left(1-\exp\left(-\lambda_n^2\tau\right)\right)}{\lambda_n^2}\right]. \tag{45}$$

3. Results and discussion

3.1. Problem parameters

In order to analyze the results from the theoretical model presented in Section 2, the values of several non-dimensional parameters must be chosen first. In general, the location of the phase change front and fraction of drug released as function of time depend on the non-dimensional parameters $\bar{\delta}$, $\bar{D}_p$, $\bar{B}$, Sh as well as the porosity ϕ. Without loss of generality, baseline values for these parameters are predominantly estimated from past work [37], which reported these values based on experimental data. The underpinning dimensional parameter values are listed in Table 1. The value of the Sherwood number depends on the nature of the release medium and mass transfer conditions at the outer surface. In general, Sh may vary from 0 to infinity, corresponding to an impenetrable and a zero concentration boundary, respectively. A baseline value of 2 is listed, but a broader range of values is considered in Section 3.6. Note that, in general, the initial drug concentration in the core is designed to be much larger than the solubility limit, and the encapsulant material is chosen to have low diffusion coefficient. These design choices facilitate control of drug release over a sustained period of time by slowing down the dissolution and diffusion processes, respectively. However, dissolution and diffusion affect each other. Therefore, the precise impact of varying these parameters is not known, and needs to be determined through systematic analysis of how these parameters impact $\bar{a}$ and $\bar{f}$, based on the theoretical model presented in the previous section. Using the baseline values of the non-dimensional parameters, a number of analyses are carried out. In order to understand the impact of each parameter on the nature of the dissolution and drug release processes, each parameter is varied at a time while holding all others constant. These are described in subsequent sub-sections.

3.2. Effect of number of eigenvalues

Given the infinite series nature of the solution, it is important to understand the minimum number of terms required in the solution, eqs. (34) and (35), to obtain reasonably accurate results. The decaying exponential term in the time domain in eqs. (34) and (35) indicates that an increasing number of terms may be needed to be computed at small times, whereas at large times, the time-dependent term in the solution may be insignificant, and only a few terms may suffice to get good accuracy. For reasonably large times, only the 'steady state' components of the solution may be sufficient, and $w_f(\xi,\tau)$ and $w_p(\xi,\tau)$ may be ignored completely. In order to investigate this for realistic settings, a number of calculations are carried out for the different numbers of terms considered. In each case, the normalized thickness of the dissolved region, $\bar{a}$ and fraction of drug released, $\bar{f}$ are computed as functions of time. As shown in plots of these quantities in Fig. 2(a) and 2(b), respectively, only a single term in the infinite series is sufficient for convergence for all considered times and for the baseline parameter set. Note that the time period for most drug delivery problems of relevance to enclosed devices

Table 1
Baseline values of various dimensional parameters of the problem considered here [27,37,38,42].

#	Parameter	Definition	Value (Units)	Source
1	D_f	Diffusion coefficient in fluid-infused core	10^{-9} (m^2s^{-1})	–
2	D_p	Diffusion coefficient of porous encapsulant	$5.1 \cdot 10^{-11}$ (m^2s^{-1})	Calculated
3	ϕ	Porosity of encapsulant	0.17	[27]
4	ϕ_e	Effective porosity	0.153	[37]
5	λ	Tortuosity	3.0	[38]
6	R_0	Radius of the drug core	1.575 (mm)	[27]
7	δ	Porous encapsulant thickness	1.6 (mm)	[27]
8	S	Solubility	3 ($kg \cdot m^{-3}$)	[42]
9	B	Initial drug concentration in core	505.19 ($kg \cdot m^{-3}$)	Calculated from [27]
10	Sh	Sherwood number	2.0	Estimated from [27]

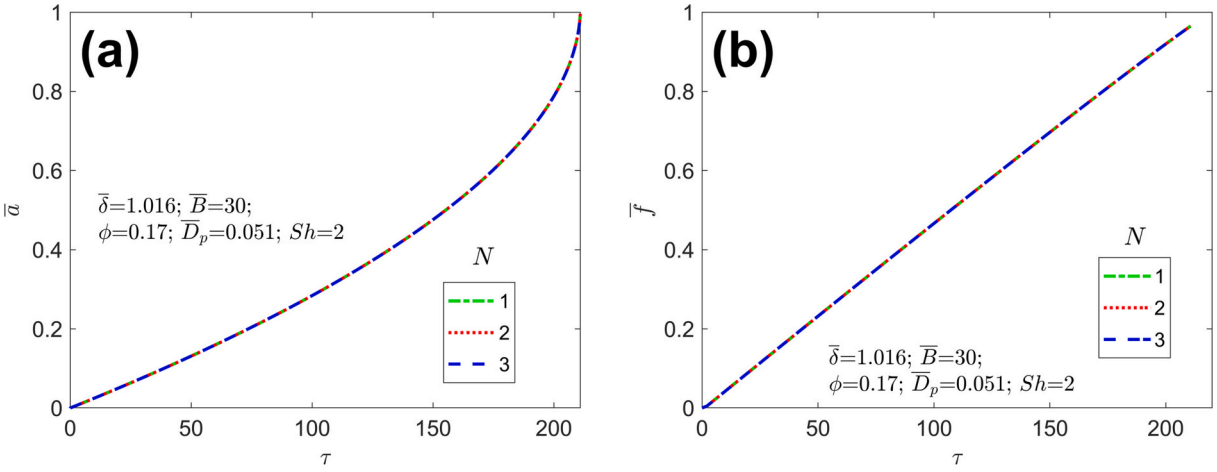

Fig. 2. Effect of number of eigenvalues, *N*, on: (a) Thickness of the dissolved drug region, and (b) fraction of drug released as functions of time for a representative problem.

considered here is quite large. For example, experimental data presented by Gimeno, et al. [27], discussed in detail in the next sub-section, is over a period of several days. Such a long time period is sufficient for transient effects to be negligible in the theoretical model. The inclusion of additional terms beyond shown in Fig. 2 does not significantly change the predicted behavior of the system. Mathematically, this occurs because even the smallest eigenvalue of this problem is sufficiently large – of the order of 1 or more – due to which, over the time periods of interest in practical applications, the transient component of eqs. (34) and (35) are negligible due to the exponentially decaying term. This results in weak dependence on the number of terms in the infinite series. From a computational perspective, this is a helpful result, since the larger the number of terms to be computed, the greater is the computational cost, particularly so in this problem, in which, the eigenvalues must be computed at each time due to the changing value of $\bar{a}$.

3.3. Model comparison with experimental data

Prior to a comprehensive analysis of a variety of drug release scenarios ranging from dissolution-limited to diffusion-limited, it is important to first demonstrate that the model is able to correctly capture experimental data. Towards this, we consider the study by Gimeno et al. [27] who measured drug release from a cylindrical drug-filled orthopedic fixation pin in an *in vitro* environment. The pins in question contained a porous wall encapsulating the solid drug core, and are, therefore, ideal for comparison with the present work. For full details of the experiment set-up and procedures, the reader is referred to [27]. Briefly, stainless steel porous-walled pins were filled with the drug Linezolid in its powdered commercial form Zyvox, then submerged in a large volume of simulated body fluid (SBF). Communication with the authors revealed that the experiment was performed under agitation. The fraction of drug released was measured at various time intervals.

The model parameters related to the geometry of the device (core radius, porous wall thickness) are available from Gimeno et al. [27]. The pins are stated as being "loaded with 95-120 mg of lyophilized commercial Linezolid." A value of 100 mg was assumed, justified from a similar study by Gimeno et al. [28], in which, precise drug loading of 100 mg is stated. The value of the free diffusion coefficient of linezolid is not, to the authors' knowledge, reported in the literature. Therefore, it is assumed that $D_f = 5 \cdot 10^{-10}$ m^{2}s^{-1}, a value broadly typical of small molecule drugs with similar molar mass. Given that the volume of the release medium is considerably larger than the volume of the pin, coupled with the fact that the experiments were performed under agitation, a high Sherwood number, effectively emulating sink conditions, is reasonable to assume.

The only remaining parameter is solubility. Gimeno et al. [27] quote the aqueous solubility of Linezolid as 3 mg/ml (= 3 kg/m^3). According to the FDA, Linezolid has an "aqueous solubility of approximately 3 mg/ml" and that Linezolid is "not ionized in aqueous media, including blood and urine, with pH>4" [42]. Additionally, according to Pfizer, the manufacturer of Zyvox (the commercial name for Linezolid), "The aqueous solubility of linezolid is approximately 3 mg/mL, independent of pH between 3 to 9." [43]. In the drug release experiments by Gimeno et al. simulated body fluid was used as the release medium, which was "prepared according to the method described by Kokubo et al. (1990)". According to Kokubo et al. [44], their simulated body fluid has a pH of 7.25, similar to human blood plasma. We note, however, that Gimeno et al. state that Zyvox "contains 2 mg of linezolid, 45.7 mg of glucose and 0.38 mg of sodium (as sodium hydroxide). The injection also contains sodium citrate, citric acid anhydrous, hydrochloric acid and water for injections". Thus, given that the formulation of linezolid used is mixed with other ingredients of higher solubility, and given that the release medium is different, we anticipate the solubility will be higher, but we are unable to quantify this *a priori*. This motivates us to treat solubility as a fitting parameter when comparing with the experimental data.

Therefore, an inverse problem is solved, whereby all known pa-

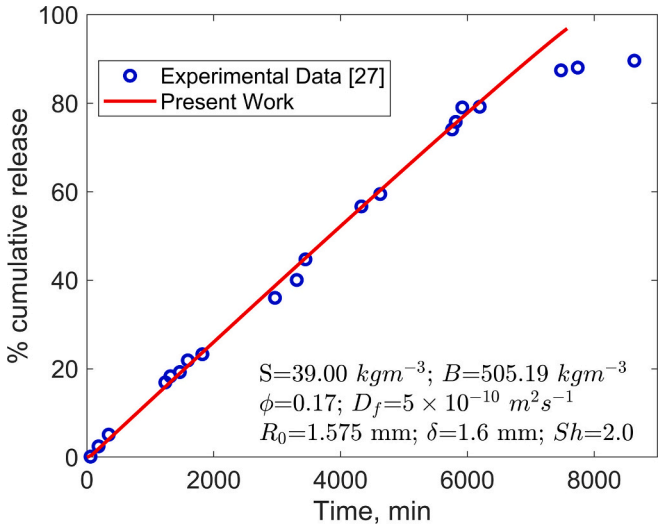

Fig. 3. Comparison of the drug release profile predicted by the theoretical model with experimental data reported by Gimeno et al. [27]. The last three experimental data points are not considered in comparison due to reasons discussed in Section 3.3.

rameters are fixed and S is varied over a physically realistic range in order to find the value that best fits experimental data. Examination of the experimental data shown in Fig. 3 reveals a largely linear drug release through most of the experiment, with a deviation from the linear trend at later times (represented by the last three data points). Given the mass of drug loaded in the device and the corresponding solubility of the drug as stated in Gimeno et al. [27], it is unlikely that this deviation arises from the release medium becoming saturated with drug (thereby reducing the concentration gradient). Rather, this behavior at later times is almost certainly a result of drug being completely dissolved and being transported through the device via diffusion only. Since the present model is focused on tracking the dissolution front until complete dissolution (i.e. it is only valid for the period up until all of the drug has been dissolved), it is not appropriate to consider these data points when comparing the model with the experimental data. Thus, the last three data points are not included in the inverse problem.

The inverse problem comprises varying S in a reasonable parametric range in order to find the value that minimizes the root-mean-square (RMS) deviation between the drug release curve predicted by the model and experimental data. The RMS error curve is found to have a minima at $S = 39.00$ kg·m^{-3}, which is the value used for comparison. It is noted that this value is higher than the reported aqueous solubility of pure linezolid, but is not unexpected, given the preceding discussion on solubility. Fig. 3 presents the drug release curve predicted by the model for this value, along with experimental data. This comparison shows that the model is able to capture the experimental data very well, exhibiting close agreement through the drug release process during dissolution. The R^2 value between experimental data and theoretical model is found to be 0.997. The very minor discrepancies between the two may be attributed to, for example, incomplete details regarding the experimental set up (which may influence Sh) and some uncertainty in the initial drug loading. Notwithstanding these minor sources of error, the overall agreement between the model and experimental data is very good.

3.4. Dissolution-vs-diffusion trade-offs

The nature of drug delivery in this problem is governed by the interplay between dissolution and diffusion, which are tightly coupled with each other. At the initial time, when the entire drug is present in solid form, no diffusion is possible within the core and, therefore, no drug release occurs. As diffusion in the encapsulant drives the inward propagation of the dissolution front, increasingly more drug becomes available for diffusion, resulting in an increase in the rate of drug released from the outer surface. Eventually, however, the concentration gradient within the device reduces, as much of the drug has already been delivered, resulting in slowdown in the rate of drug delivered. The rate of diffusion drives the dissolution process. In turn, the dissolution process enables diffusion by rendering more and more drug diffusible. Due to the close coupling between the two processes, the governing non-dimensional parameters of this problem must be carefully chosen on the basis of the influence of these parameters on both dissolution and diffusion, and eventually on the drug release profile.

In order to carefully investigate these coupled processes, the impact of the initial drug distribution, represented by the non-dimensional parameter $\bar{B}$ on dissolution-limited drug delivery characteristics is investigated first. For baseline values of other parameters, Fig. 4(a) plots the dissolution front as a function of time for different values of $\bar{B}$. Note that large values of $\bar{B}$ are chosen in order to be consistent with past literature [27,28,38], where a large excess of drug is made available initially. Fig. 4(a) shows, as expected, that the propagation of the dissolution front begins very slowly, and then speeds up. This arises because of the slow rate of diffusion at early times, whereas at later times, the amount of drug remaining in the solid form reduces, making it easier to dissolve. The latter phenomenon explains the very sharp nature of the dissolution front propagation curves towards the end of the process. Fig. 4(a) also demonstrates strong dependence of the dissolution process on the initial concentration $\bar{B}$. The greater the initial drug loading, the slower is the dissolution process, because for the same diffusive flux driving the dissolution process, per eq. (15), a larger value of $\bar{B}$ results in lower value of $d\bar{a}/dt$. Due to the appearance of $\bar{B}$ in the denominator of eq. (15), a strong dependence of the dissolution process on $\bar{B}$ may be expected, which is confirmed by Fig. 4(b), which plots the total dissolution time (i.e., the time taken until all of the drug has dissolved) as a function of $\bar{B}$. Fig. 4(b) shows, as expected, that the total dissolution time increases linearly with $\bar{B}$.

Fig. 5 investigates the impact of $\bar{B}$ on the cumulative amount of drug released from the device, $\bar{f}$, until the end of the dissolution process (i.e. until all of the drug within the core has dissolved). Fig. 5(a) plots $\bar{f}$ as a function of τ, up to the corresponding time for complete dissolution, for different values of $\bar{B}$ while all other parameters are held constant. Consistent with past measurements [27], a zero-order release is observed (i.e. $\bar{f}$ increases linearly with time), which may be because the drug reservoir system is loaded high above the solubility limit. It is particularly interesting that the total amount of drug delivered by the end of the dissolution process increases with increasing value of $\bar{B}$. This is primarily because larger values of $\bar{B}$ result in slower dissolution, giving more time for the drug to diffuse and be delivered on the outer surface. This is further illustrated in Fig. 5(b), which plots the total

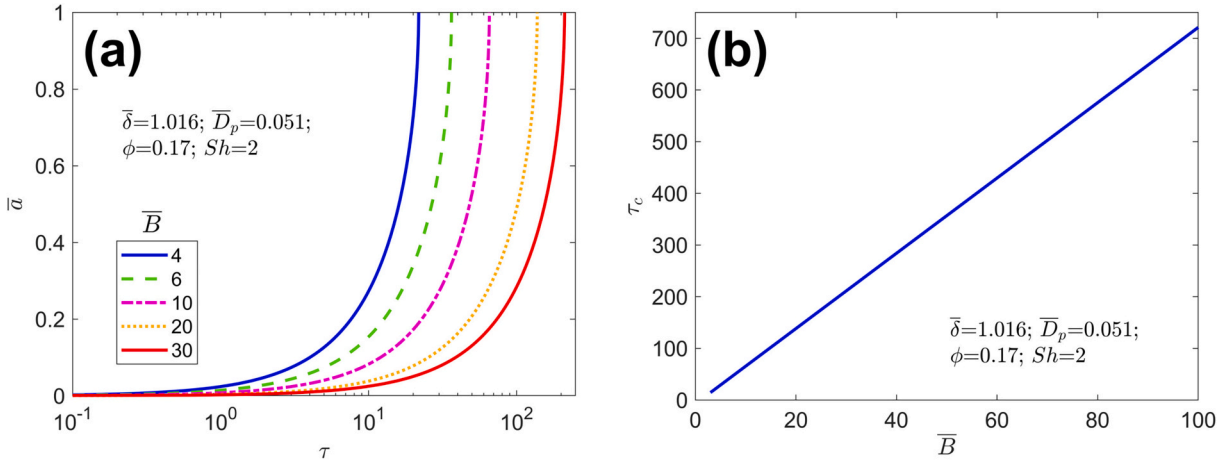

Fig. 4. Effect of non-dimensional initial drug concentration on dissolution process: (a) Dissolution front propagation as a function of τ for different values of $\bar{B}$, and (b) total dissolution time, τ_c as a function of $\bar{B}$.

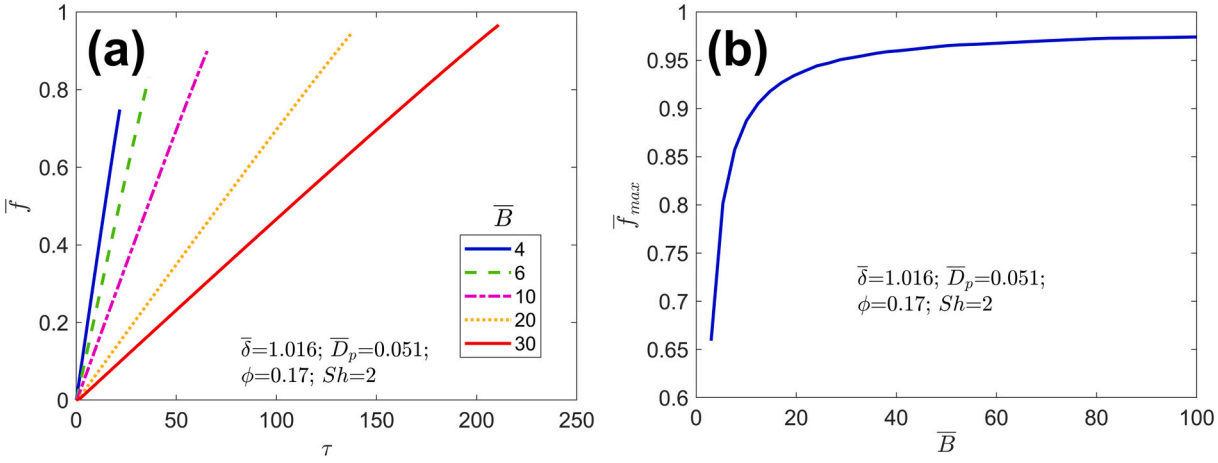

Fig. 5. Effect of non-dimensional initial concentration on drug release: (a) Fraction of drug delivered as a function of time until the end of the dissolution process for different values of $\bar{B}$, and (b) Total fraction of drug delivered by the end of the dissolution process as a function of $\bar{B}$.

fraction of drug delivered by the end of the dissolution process, $\bar{f}_{max}$ as a function of $\bar{B}$. As expected, this plot shows rapid increase in $\bar{f}_{max}$ with increasing $\bar{B}$ at small values of $\bar{B}$, whereas, this effect saturates at a value close to 1 for large $\bar{B}$. This is likely because when $\bar{B}$ is sufficiently large, the dissolution process is occurring so slowly – with diffusion relatively rapid – that almost all the drug is delivered by the time dissolution is complete. The other extreme situation is when $\bar{B}$ is very close to 1, in which case, dissolution occurs very rapidly, and the drug delivery characteristics are largely governed by diffusion of fully dissolved drug in the device. Drug delivery in this diffusion-limited regime has been modeled extensively in past papers [1,3,21,45].

In light of the discussion above, $\bar{B}$ is identified as a key non-dimensional parameter that governs the interplay between dissolution and diffusion in this problem, therefore strongly influencing drug delivery characteristics, which is usually of much practical interest.

3.5. Effect of encapsulant properties

The porous encapsulant around the drug core is expected to play a key role in drug release, since drug release at the outer surface is mediated by diffusion through the encapsulant layer. While in practice, the encapsulant may be designed to provide mechanical strength, yet, too thick an encapsulant is intuitively expected to result in slowdown of the drug release process, which, in some cases, may be desirable, and in other cases, undesirable. The two key properties of the porous encapsulant that appear in the mathematical model presented here include the thickness and the effective diffusion coefficient of drug within the encapsulant. These are captured within the non-dimensional parameters $\bar{\delta}$ and $\bar{D}_p$, respectively, both of which are expressed relative to that of the respective property of the drug core.

The effect of these parameters on the dissolution front propagation and drug release profile is investigated. Firstly, Fig. 6(a) plots the thickness of the dissolved drug region $\bar{a}$ as a function of time for four different encapsulant thicknesses, while all other parameters are held constant. A plot of the cumulative fraction of drug released, $\bar{f}$, as a function of time for the same set of parameters is presented in Fig. 6(b). Fig. 6(a) shows that as the encapsulant thickness increases, the dissolution front propagates slower and slower. This is explainable on the basis of greater resistance to diffusion offered by a thick encapsulant layer. The reduced dissolution propagation at large thicknesses is particularly noticeable at small times, which is because the initial diffusion of dissolved drug from the initial dissolution front at $r = R_0$ through the thicker encapsulant will take longer. Fig. 6(b) shows that as the encapsulant thickness increases, the drug takes longer to release, however, the total drug released by the end of the dissolution process remains approximately the same, regardless of the encapsulant thickness. This may seem counter-intuitive at first, but is likely due to the dependence of the speed of dissolution on diffusion. In other words,

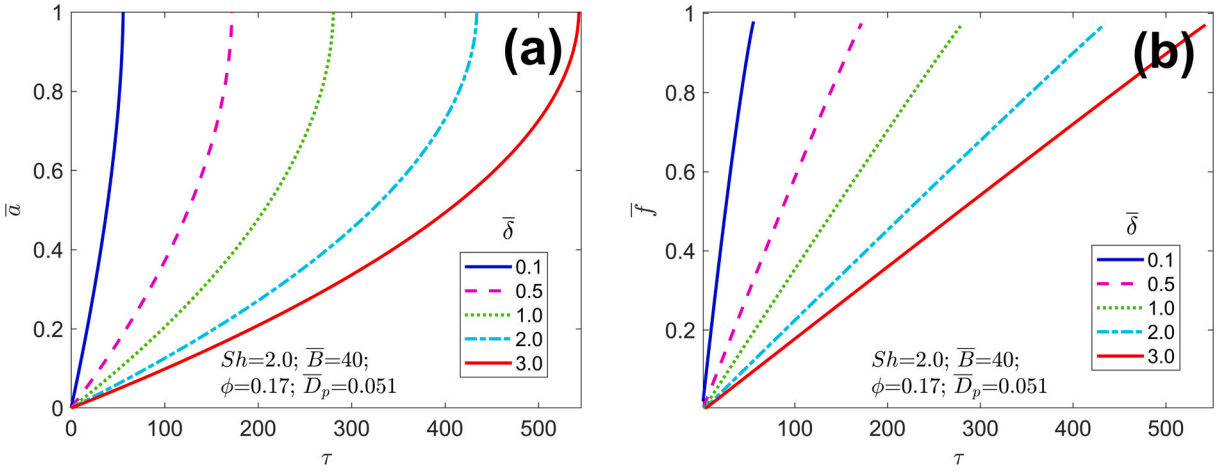

Fig. 6. Effect of porous wall thickness: (a) time-varying thickness of the dissolved drug region and (b) cumulative drug released as a function of time. Both are plotted for multiple values of the porous wall thickness.

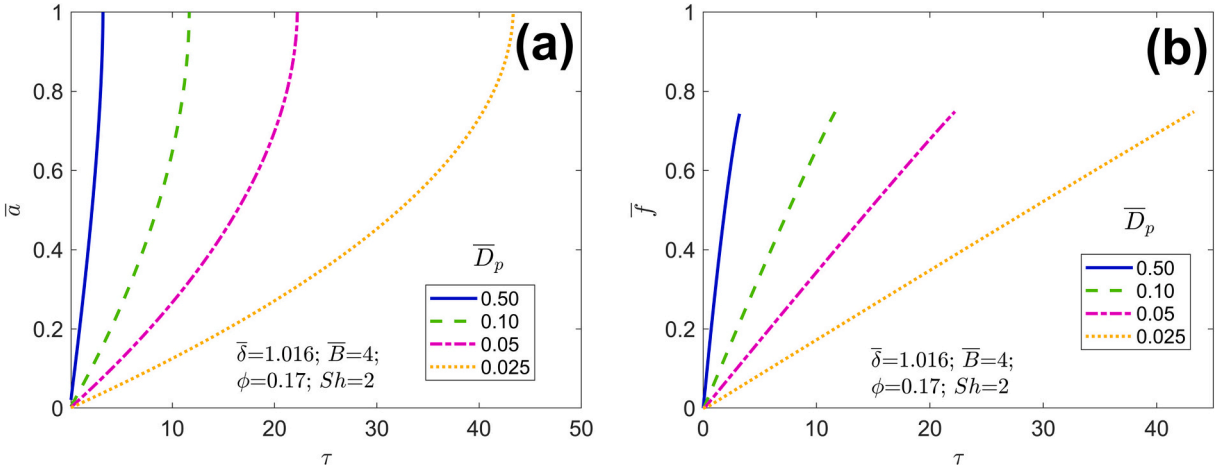

Fig. 7. Effect of porous wall diffusion coefficient: (a) time-varying thickness of the dissolved drug region and (b) cumulative drug released as a function of time. Both are plotted for multiple values of the porous wall diffusion coefficient.

while increased encapsulant thickness increases the timescale for diffusion, at the same time it slows down dissolution, thereby providing more time for drug to diffuse and release on the outer surface while dissolution is still ongoing.

The impact of the other key non-dimensional parameter related to the encapsulant, $\bar{D}_p$, is presented in Fig. 7. For four different values of $\bar{D}_p$, Figs. 7(a) and 7(b) plot the thickness of the dissolved drug region $\bar{a}$ and fraction of drug released $\bar{f}$ as functions of time. As expected, the lower the value of $\bar{D}_p$, the slower diffusion is through the encapsulant, and, therefore, the slower is the inwards propagation of the dissolution front. Changing $\bar{D}_p$ does not appear to influence the fraction of drug released by the end of the dissolution process, with a rationale similar to that for the effect of changing the encapsulant thickness $\bar{\delta}$. Note that, in contrast with the $\bar{\delta}$ case presented in Fig. 6(b), where almost all of the drug had been released by the end of the dissolution process, in this case, notably less drug has been released by the end of the dissolution process for each of the values of $\bar{D}_p$ considered here. This implies that under the parameter values of Fig. 6, the drug delivery process is not dissolution-limited, and that a sizable portion of dissolved drug still remains within the core and encapsulant by the time the drug core is completely dissolved. Note that a key difference between the parameter sets for Figs. 6 and 7 is that the value of the initial concentration is $\bar{B}$ is 40 and 4.0, respectively. As discussed in the previous section, $\bar{B}$ strongly influences whether the process is diffusion or dissolution limited, which explains the difference in the nature of Figs. 6(b) and 7(b). In contrast with $\bar{B}$, the encapsulant properties $\bar{\delta}$ and $\bar{D}_p$ do not play a key role in determining whether dissolution or diffusion dominates primarily because, unlike $\bar{B}$, which only influences the dissolution process via eq. (15), $\bar{\delta}$ and $\bar{D}_p$ equally influence both dissolution and diffusion.

When the drug release during the inwards propagation of the dissolution front is diffusion-limited, such as in Fig. 7, subsequent delivery of the remaining drug after completion of dissolution is driven by a pure diffusion process, which, for multilayer geometries similar to the present work has been addressed in past work [6,29,30,45], and, therefore, is not considered here. It is to be noted that the drug concentration profile in the core and encapsulant at the end of the dissolution process, i.e., $\tau = \tau_c$, serves as the initial condition for the transient diffusion process that describes the remaining drug delivery process post-dissolution.

Given the importance of the time for complete dissolution, particularly for modeling the remaining drug release post-dissolution in the case of a diffusion-limited process, the impact of encapsulant properties on the total dissolution time is investigated next. Keeping other parameters fixed, the time for complete dissolution τ_c is plotted as a function of encapsulant thickness and encapsulant diffusion coefficient in Figs. 8(a) and 8(b), respectively. In each case, curves are plotted for two values of the initial drug concentration, $\bar{B} = 40.0$ and $\bar{B} = 4.0$, that represent dissolution-limited and diffusion-limited regimes, respectively. Fig. 8(a) shows, as expected, an increase in τ_c with increase in $\bar{\delta}$ due to the greater resistance to diffusion offered by the thicker

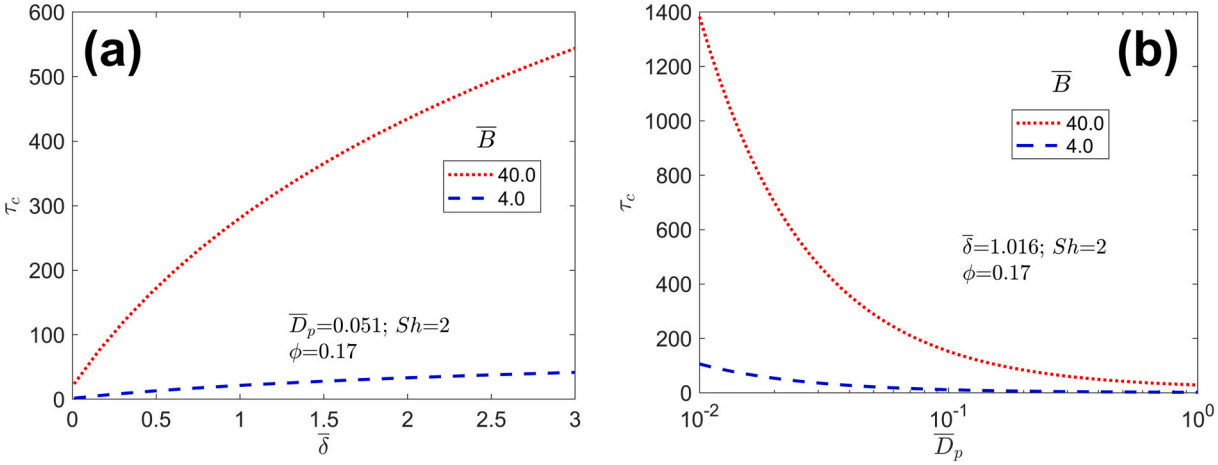

Fig. 8. Time for complete dissolution as a function of (a) porous wall thickness and (b) porous wall diffusion coefficient.

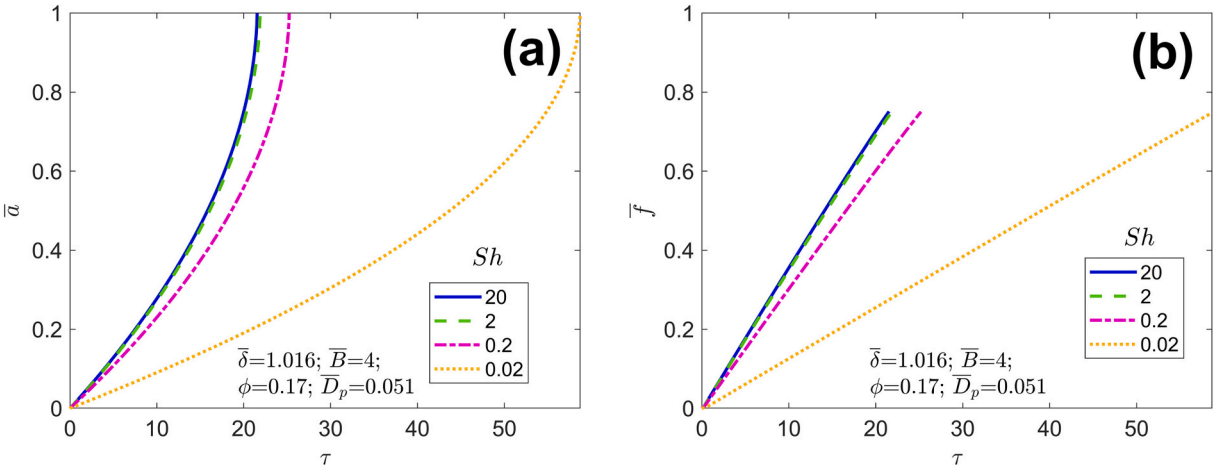

Fig. 9. Effect of Sherwood number: (a) thickness of dissolved drug region and (b) fraction of drug released as functions of time for different values of the Sherwood number.

encapsulant. The increase, however, is self-limiting, and the curve in Fig. 8(a) is seen to slow down somewhat at large thicknesses, at which point, the encapsulant is already very thick, so that the effect of further increase in thickness is relatively weaker than when the encapsulant is thinner.

In contrast, the effect of encapsulant diffusion coefficient $\bar{D}_p$ shown in Fig. 8(b) indicates that $\bar{D}_p$ has much stronger impact on the time for complete dissolution. Particularly at very small values of the diffusion coefficient, the time taken for dissolution to complete increases dramatically with $\bar{D}_p$. This is mainly because extremely small $\bar{D}_p$ implies very large resistance to diffusion, and, therefore, very slow propagation of the dissolution front. Unlike the effect of $\bar{\delta}$ shown in Fig. 8(a), $\bar{D}_p$ appears to have a much stronger impact on the time for complete dissolution.

In both Figs. 8(a) and 8(b), the impact of encapsulant properties on dissolution time is similar, regardless of whether the process is dissolution-limited ($\bar{B} = 40.0$) or diffusion-limited ($\bar{B} = 4.0$). As expected, the time for complete dissolution is lower in both cases when diffusion-limited, because a small initial concentration results in a faster-propagating dissolution front, per eq. (15).

3.6. Effect of external conditions

The impact of the external boundary condition at $\xi = 1 + \bar{\delta}$ on dissolution front propagation and drug release is examined next. The nature of the external boundary is mathematically represented by the Sherwood number, *Sh*. A very small value of *Sh* represents an impermeable condition, whereas a large value of *Sh* represents an infinite sink, resulting in zero drug concentration at the external boundary. Figs. 9(a) and 9(b) plot the thickness of the dissolved drug region $\bar{a}$ and fraction of drug released $\bar{f}$ as functions of time for multiple values of *Sh* spanning this spectrum. As expected, it is found that *Sh* impacts the dissolution and, consequently, drug release process. At small *Sh*, only limited amount of drug can be released from the outer surface, which slows down both dissolution and drug release. The dissolution is affected because, per eq. (15), the propagation of the dissolution front is driven by outwards diffusion of the drug from the dissolution front towards the outer surface, which is severely throttled when *Sh* is small. As *Sh* increases, the $\bar{a}$ curves become steeper and steeper, indicating faster dissolution. However, a saturation effect exists, in that increasing *Sh* beyond a threshold results in only incremental increase in the rate of dissolution. This is likely because once the external boundary is sufficiently conducive to drug loss to the ambient, the rate-limiting step shifts to diffusion within the core and porous encapsulant, implying that further increasing *Sh* does not significantly affect the dissolution process. Similar to Figs. 6(b) and 7(b) related to encapsulant properties, Fig. 9(b) indicates that changing *Sh* does not influence the total fraction of drug released up to the end of dissolution process, because this primarily depends on whether the process is dissolution-limited or diffusion-limited, which, as shown previously, is governed primarily by the initial concentration $\bar{B}$.

4. Conclusions

This work develops a mathematical model that describes controlled release from a drug-loaded cylindrical device surrounded by a passive porous layer. The analysis presented here uncovers how the various geometrical and physicochemical parameters influence drug dissolution and, ultimately, the drug release profile. Key non-dimensional parameters that influence the drug delivery process are identified. The model is compared against experimental data available in the literature, and excellent agreement is found, thereby providing confidence in its predictive capabilities.

The derivation of the theoretical model is based on the principle of mass conservation during an inwards propagating dissolution front. The derivation does not rely on results or data from a specific past experiment, and, therefore, is not empirical in nature. As long as the underlying assumptions of the model (such as a reasonably slow-moving dissolution front, so that the problem is not heavily diffusion-limited) remain valid, the model predictions are expected to retain accuracy.

The fundamental theoretical principles used here may be extended to different geometrical configurations and numbers of encapsulating layers with potentially different properties. It is expected that the model will be useful for those designing such devices, in terms of optimizing the design of the device to achieve a desired drug release profile.

CRediT authorship contribution statement

Ankur Jain: Writing – review & editing, Writing – original draft, Validation, Supervision, Project administration, Methodology, Investigation, Formal analysis, Data curation, Conceptualization. **David King:** Writing – review & editing, Writing – original draft, Validation, Investigation. **Giuseppe Pontrelli:** Writing – review & editing, Writing – original draft, Validation, Methodology, Formal analysis, Conceptualization. **Sean McGinty:** Writing – review & editing, Writing – original draft, Validation, Methodology, Formal analysis, Conceptualization.

Data accessibility

All data supporting this study are provided within the main text.

Acknowledgments

David King would like to gratefully acknowledge the funding provided by EPSRC (grant number EP/M506539/1). Sean McGinty acknowledges funding provided by EPSRC (grant number EP/S030875/1). Giuseppe Pontrelli acknowledges funding from the European Research Council under the European Unions Horizon 2020 Framework Programme (No. FP/2014–2020)/ ERC Grant Agreement No. 739964 (COPMAT).

References

[1] J. Siepmann, F. Siepmann, Mathematical modelling of drug delivery, Int. J. Pharm. 364 (2008) 328–343, https://doi.org/10.1016/j.ijpharm.2008.09.004.
[2] J. Siepmann, F. Siepmann, Mathematical modelling of drug dissolution, Int. J. Pharm. 453 (2013) 12–24, https://doi.org/10.1016/j.ijpharm.2013.04.044.
[3] D.Y. Arifin, L.Y. Lee, C.-H. Wang, Mathematical modeling and simulation of drug release from microspheres: Implications to drug delivery systems, Adv. Drug Deliv. Rev. 58 (2006) 1274–1325, https://doi.org/10.1016/j.addr.2006.09.007.
[4] G.G. Stefanini, D.R. Holmes, Drug-eluting coronary artery stents, N. Engl. J. Med. 368 (2013) 254–265, https://doi.org/10.1056/NEJMra1210 816.
[5] M.R. Prausnitz, R. Langer, Transdermal drug delivery, Nat. Biotechnol. 26 (2008) 1261–1268, https://doi.org/10.1038/nbt.1504.
[6] A. Jain, K. Subbarao, S. McGinty, G. Pontrelli, Optimization of initial drug distribution in spherical capsules for personalized release, Pharm. Res. 39 (2022) 2607–2620, https://doi.org/10.1007/s11095-022-03359-y.
[7] A.A. Noyes, W.R. Whitney, The rate of solution of solid substances in their own solutions, J. Am. Chem. Soc. 19 (1897) 930–934, https://doi.org/10.1021/ja02086a003.
[8] T. Higuchi, Rate of release of medicaments from ointment bases containing drugs in suspension, J. Pharm. Sci. 50 (1961) 874–875, https://doi.org/10.1002/jps.2600501018.
[9] A.W. Hixson, J.H. Crowell, Dependence of reaction velocity upon surface and agitation, Ind. Eng. Chem. 23 (1931) 923–931, https://doi.org/10.1021/ie50260a018.
[10] W. Nernst, Theorie der Reaktionsgeschwindigkeit in heterogenen Systemen, Z. Phys. Chem. 47 (1904) 52–55, https://doi.org/10.1515/zpch-1904-4704.
[11] P.I. Lee, Modeling of drug release from matrix systems involving moving boundaries: approximate analytical solutions, Int. J. Pharm. 418 (2011) 18–27, https://doi.org/10.1016/j.ijpharm.2011.01.019.
[12] B. Narasimhan, Mathematical models describing polymer dissolution: consequences for drug delivery, Adv. Drug Deliv. Rev. 48 (2001) 195–210, https://doi.org/10.1016/S0169-409X(01)00117-X.
[13] G. Frenning, Modelling drug release from inert matrix systems: from moving-boundary to continuous-field descriptions, Int. J. Pharm. 418 (2011) 88–99, https://doi.org/10.1016/j.ijpharm.2010.11.030.
[14] M. Meere, G. Pontrelli, S. McGinty, Modelling phase separation in amorphous solid dispersions, Acta Biomater. 94 (2019) 410–424, https://doi.org/10.1016/j.actbio.2019.06.009.
[15] T. Vo, S. Morgan, C. McCormick, S. McGinty, S. McKee, M. Meere, Modelling drug release from polymer-free coronary stents with microporous surfaces, Int. J. Pharm. 544 (2018) 392–401, https://doi.org/10.1016/j.ijpharm.2017.12.007.
[16] K.M. Moroney, M. Vynnycky, Mathematical modelling of drug release from a porous granule, Appl. Math. Model. 100 (2021) 432–452, https://doi.org/10.1016/j.apm.2021.07.023.
[17] K.M. Moroney, L. Kotamarthy, I. Muthancheri, R. Ramachandran, M. Vynnycky, A moving-boundary model of dissolution from binary drug-excipient granules incorporating microstructure, Int. J. Pharm. 599 (2021), 120219, https://doi.org/10.1016/j.ijpharm.2021.120219.
[18] T. Higuchi, Mechanism of sustained-action medication: theoretical analysis of rate of release of solid drugs dispersed in solid matrices, J. Pharm. Sci. 52 (1963) 1145–1149, https://doi.org/10.1002/jps.2600521210.
[19] P.I. Lee, Diffusional release of a solute from a polymeric matrix—approximate analytical solutions, J. Membr. Sci. 7 (1980) 255–275, https://doi.org/10.1016/S0376-7388(00)80472-X.
[20] T. Koizumi, M. Ueda, M. Kakemi, H. Kameda, Rate of release of medicaments from ointment bases containing drugs in suspension, Chem. Pharm. Bull. 23 (1975) 3288–3292, https://doi.org/10.1002/jps.2600501018.
[21] S. McGinty, G. Pontrelli, A general model of coupled drug release and tissue absorption for drug delivery devices, J. Control. Release 217 (2015) 327–336, https://doi.org/10.1016/j.jconrel.2015.09.025.
[22] G. Frenning, Theoretical investigation of drug release from planar matrix systems: effects of a finite dissolution rate, J. Control. Release 92 (2003) 331–339, https://doi.org/10.1016/S0168-3659(03)00338-9.
[23] D. King, C. McCormick, S. McGinty, How does fluid flow influence drug release from drug filled implants, Pharm. Res. 39 (2022) 25–40, https://doi.org/10.1007/s11095-021-03127-4.
[24] E. Brunner, Reaktionsgeschwindigkeit in heterogenen Systemen, Z. Phys. Chem. 47 (1904) 56–102, https://doi.org/10.1515/zpch-1904-4705.
[25] R.S. Harland, C. Dubernet, J.P. Benoit, N.A. Peppas, A model of dissolution-controlled, diffusional drug release from nonswellable polymeric microspheres, J. Control. Release 7 (1988) 207–215, https://doi.org/10.1016/0168-3659(88)90053-3.
[26] S.G. Worthley, A. Abizaid, A. Kirtane, D. Simon, S. Windecker, S. Brar, I. Meredith, S. Shetty, A. Sinhal, A. Almonacid, D. Chamie, A. Maehara, G.W. Stone, First-in-human evaluation of a novel polymer-free drug-filled stent: Angiographic, IVUS, OCT, and clinical outcomes from the RevElution study, J. Am. Coll. Cardiol. Intv. 10 (2017) 147–156, https://doi.org/10.1016/j.jcin.2016.10.020.
[27] M. Gimeno, P. Pinczowski, F. Vázquez, M. Pérez, J. Santamaŕıa, M. Arruebo, L. Luján, Porous orthopedic steel implant as an antibiotic eluting device: prevention of post-surgical infection on an ovine model, Int. J. Pharm. 452 (2013) 166–172, https://doi.org/10.1016/j.ijpharm.2013.04.076.
[28] M. Gimeno, P. Pinczowski, M. Pérez, A. Giorello, M. Martínez, J. Santamaŕıa, M. Arruebo, L. Luján, A controlled antibiotic release system to prevent orthopedic-implant associated infections: an in vitro study, Eur. J. Pharm. Biopharm. 96 (2015) 264–271, https://doi.org/10.1016/j.ejpb.2015.08.007.
[29] A. Jain, M. Parhizi, Theoretical analysis of phase change heat transfer and energy storage in a spherical phase change material with encapsulation, Int. J. Heat Mass Transf. 185 (2022) 122348, 1-12, https://doi.org/10.1016/j.ijheatmasstransfer.2021.122348, 1-12.
[30] M. Parhizi, A. Jain, Theoretical modeling of solid-liquid phase change in a phase change material protected by a multilayer Cartesian wall, Int. J. Heat Mass Transf. 197 (2022) 123330, 1-16, https://doi.org/10.1016/j.ijheatmasstransfer.2022.123330, 1-16.
[31] E. Kaunisto, S. Abrahmsen-Alami, P. Borgquist, A. Larsson, B. Nilsson, A. Axelsson, A mechanistic modelling approach to polymer dissolution using magnetic resonance microimaging, J. Control. Release 147 (2010) 232–241, https://doi.org/10.1016/j.jconrel.2010.07.102.
[32] E. Kaunisto, M. Marucci, A. Axelsson, Dissolution kinetics or pure mass transfer? A mechanistic study of dissolution, AICHE J. 57 (2011) 2610–2617, https://doi.org/10.1002/aic.12475.
[33] E. Kaunisto, M. Marucci, P. Borgquist, A. Axelsson, Mechanistic modelling of drug release from polymer-coated and swelling and dissolving polymer matrix systems, Int. J. Pharm. 418 (2011) 54–77, https://doi.org/10.1016/j.ijpharm.2011.01.021.
[34] E. Kaunisto, F. Tajarobi, S. Abrahmsen-Alami, A. Larsson, B. Nilsson, A. Axelsson, Mechanistic modelling of drug release from a polymer matrix using magnetic resonance microimaging, Eur. J. Pharm. Sci. 48 (2013) 698–708, https://doi.org/10.1016/j.ejps.2012.12.030.
[35] J. Crank, The Mathematics of Diffusion, 2nd Ed, Oxford Science Publications, 1980.
[36] M. Abrami, L. Grassi, R. di Vittorio, D. Hasa, B. Perissutti, D. Voinovich, G. Grassi, I. Colombo, M. Grassi, Dissolution of an ensemble of differently shaped poly-dispersed drug particles undergoing solubility reduction: mathematical modelling, ADMET & DMPK 8 (2020) 297–313, https://doi.org/10.5599/admet.841.
[37] D.J. King, Controlled release of therapeutics from orthopaedic implants, Ph.D. thesis,, University of Glasgow, 2020.
[38] E.L. Cussler, Diffusion: Mass Transfer in Fluid Systems, 3rd edition, Cambridge University Press, 2009.
[39] V. Alexiades, A.D. Solomon, Mathematical Modeling of Melting and Freezing Processes, Routledge, 1993, https://doi.org/10.1201/9780203749449.
[40] G. Krishnan, M. Parhizi, A. Jain, Eigenfunction-based solution for solid-liquid phase change heat transfer problems with time-dependent boundary conditions, Int. J. Heat Mass Transf. 189 (2022) 122693, 1-12, https://doi.org/10.1016/j.ijheatmasstransfer.2022.122693, 1-12.
[41] M. Parhizi, A. Jain, Eigenfunction-based solution for one-dimensional solid-liquid phase change heat transfer problems with advection, Int. J. Therm. Sci. 172 (2022) 107262, 1-11, https://doi.org/10.1016/j.ijthermalsci.2021.107262.
[42] https://www.accessdata.fda.gov/drugsatfda_docs/nda/2000/21130_Zyvox_biopharmr.pdf accessed May 24, 2023.
[43] https://rss.medsinfo.com.au/pf/pi.cfm?product=pfpzyvoa accessed May 24, 2023.
[44] T. Kokubo, H. Kushitani, S. Sakka, T. Kitsugi, T. Yamamuro, Solutions able to reproduce in vivo surface-structure changes in bioactive glass-ceramic A-W, J. Biomed. Mater. Res 24 (1990) 721–734, https://doi.org/10.1002/jbm.820240607.
[45] A. Jain, S. McGinty, G. Pontrelli, L. Zhou, Theoretical modeling of endovascular drug delivery into a multilayer arterial wall from a drug-coated balloon, Int. J. Heat Mass Transf. 187 (2022) 122572, 1-17, https://doi.org/10.1016/j.ijheatmasstransfer.2022.122572.